Effect of Various Parameters on the Flapping Motion of an Aerofoil

Sharanappa V. Sajjan[1], K. Siva Kumar[2]

[1] Computational and Theoretical Fluid Dynamics Division, [2] Council of Scientific and Industrial Research, National Aerospace Laboratories
Bangalore, Karnataka, India

[1]svsajjan@ctfd.cmmacs.ernet.in; [2]shivak@ctfd.cmmacs.ernet.in

Abstract

Unsteady Reynolds-averaged Navier-Stokes (RANS) computations are presented for the flow past a flapping NACA 0012 aerofoil to study the effect of various motion parameters on the propulsive efficiency and thrust coefficient. The RANS solver used to obtain the time-accurate solutions is based on an implicit dual time stepping scheme with finite volume nodal point spatial discretization. The algebraic eddy viscosity model due to Baldwin and Lomax is used for the turbulence closure. The motion parameters considered are reduced frequency, amplitude of the pitch and plunge motions and phase shift between them. The computed results compare well with the available data in the literature.

Keywords

Unsteady Flow; RANS Solver; Implicit Method; Dual Time Stepping; Flapping Aerofoil

Introduction

In recent years, Micro Air Vehicles (MAVs), Unmanned Air Vehicles (UAV's) and Nano Air Vehicles (NAV's) are becoming increasingly important, especially in the area of military/defence surveillance. These are classified into fixed, rotary and flapping wing air vehicles. At low range Reynolds number, flapping wings are more efficient and more easily manoeuvrable compared to fixed wings. Numerous computational as well as experimental studies have been conducted to investigate the kinematics and dynamics of flapping wings.

Many important features of flapping aerofoil behaviour are depicted by the classical linear theory. Theodorsen developed compact expressions for forces and moments of a flapping aerofoil under the assumption of small perturbation for inviscid and incompressible flow. The flow is divided into two classes: the non-circulating flow and the circulatory flow due to wake vortices. The thrust force and the power input experienced by the flapping aerofoil were given by Garrick . Ho and Chen studied the unsteady wake of a plunging Aerofoil NACA 0012 in a low turbulence wind- tunnel by a miniature multiple hot-wire probe at Reynolds number ($2.1 \times 10^4 \sim 10^5$), reduced frequency (0 to 1), and mean angle of attack 5°. Under the condition of no dynamic stall, the near wake consists of viscous and inviscid parts. The viscous wake is, the result of the merging of two boundary layers on the aerofoil, has high velocity gradient and turbulence levels, and is limited to a very thin region. The inviscid wake is caused by the induced flow of the circulation around the plunging aerofoil and is laminar and of large width. Anderson and Anderson et al. have obtained visualization and force data for a plunging and pitching aerofoil moving in a water tank facility over a large range of amplitudes, frequencies, and phase angles. Propulsive efficiency, as high as 87% is measured experimentally under conditions of optimal wake formation. They found that agreement between the experimental data and numerical predictions of a non linear incompressible unsteady potential-flow method is good when either very weak or no flow separation vortices forms. Isogai et al. simulated dynamic stall phenomena around a flapping NACA 0012 aerofoil by a Navier-Stokes code at a free stream Mach number of 0.3 and Reynolds number of 10^5. The Baldwin and Lomax algebraic turbulence model is used in the computation. They found that high propulsive efficiency occurs for the case in which the pitching oscillation advances 90 degree ahead of the plunging oscillation and the reduced frequency is at some optimum value, for which there appears no appreciable flow separation in spite of large-amplitude oscillations.

IMPRANS Solver

The solver is based on an implicit finite volume nodal point spatial discretization scheme with dual time stepping. Inviscid flux vectors are calculated by using the flow variables at the six neighbouring points of hexahedral volume. Turbulence closure is achieved through the algebraic eddy viscosity model of Baldwin and Lomax .

The two-dimensional Reynolds averaged Navier-Stokes equations for a moving domain can be written in non-dimensional conservative form as

$$\frac{\partial U}{\partial t}+\frac{\partial F}{\partial x}+\frac{\partial G}{\partial y}=\frac{\partial V}{\partial x}+\frac{\partial W}{\partial y} \tag{1}$$

Here x and y are the Cartesian coordinates and t is the time while $\dot{x}$ and $\dot{y}$ are the Cartesian velocity components of the moving domain. For a fixed domain, the gird speeds $\dot{x}$ and $\dot{y}$ are zero. U is the vector of conserved variables; F, G are inviscid flux vectors and V, W are viscous flux vectors.

Applying Euler's implicit time differencing formula

$$U^{n}=U^{n+1}-\left(\frac{\partial U}{\partial t}\right)^{n+1}\Delta t+O\left(\Delta t^{2}\right) \tag{2}$$

to the governing Eq. (1), we obtain

$$\Delta U^{n}+\Delta t\left[\frac{\partial}{\partial x}\left(F-V\right)+\frac{\partial}{\partial y}\left(G-W\right)\right]^{n+1}=0 \tag{3}$$

Here $U^{n} = U(t) = U(n\,\Delta t)$ is the solution vector at time level n and $\Delta U^{n} = (U^{n+1} - U^{n})$ is the change in U^{n} over time step Δt. In order to facilitate the finite volume formulation, the above equations are written in the integral form as

$$\iint_{\Omega}\Delta U^{n}dxdy+\Delta t\int_{\Gamma}\left[\left(F-V\right)^{n+1}dy-\left(G-W\right)^{n+1}dx\right]=0 \tag{4}$$

where Ω is any two-dimensional flow domain and Γ is the boundary curve.

In the nodal point finite volume approach, the flow variables are associated with each mesh point of the grid and the integral conservative equations are applied to each control volume obtained by joining the centroids of the four neighbouring cells of a nodal point.

Application of nodal point spatial discretization to Eq. (4) leads to the following equations for the computational cell Ω_{ij}

$$\Delta U_{ij}^{n}h_{ij}+\Delta t\int_{\Gamma_{ij}}\left[\left(F-V\right)^{n+1}dy-\left(G-W\right)^{n+1}dx\right]=0 \tag{5}$$

where h_{ij} is the area of quadrilateral and the integral refers to a contour integration around the boundary Γ_{ij} of the cell Ω_{ij} in anticlockwise direction. The fluxes are calculated across the four sides of the control volume.

Linearising the changes in flux vectors using Taylor's series expansions in time and assuming locally constant transport properties, Eq. (5) can be simplified to

$$\begin{aligned}&\Delta U_{ij}^{n}+\frac{\Delta t}{h_{ij}}\left[\int_{\Gamma_{ij}}\left\{A^{n}-\frac{\partial}{\partial x}R^{n}\right\}\Delta U^{n}dy-\int_{\Gamma_{ij}}\left\{B^{n}-\frac{\partial}{\partial y}S^{n}\right\}\Delta U^{n}dx\right]\\&=-\frac{\Delta t}{h_{ij}}\left[\int_{\Gamma_{ij}}\left(F-V\right)^{n}dy+\int_{\Gamma_{ij}}\left(G-W\right)^{n}dx\right]\end{aligned} \tag{6}$$

Here A, B, R and S are the Jacobian matrices given by

$$A=\frac{\partial F}{\partial U},\ B=\frac{\partial G}{\partial U},\ R=\frac{\partial V_{1}}{\partial U_{x}}\ \text{and}\ S=\frac{\partial W_{2}}{\partial U_{y}} \tag{7}$$

The algebraic eddy viscosity model due to Baldwin and Lomax is used for turbulence closure. This RANS solver has been extensively validated for computing unsteady flow past pitching aerofoils and wings, plunging aerofoils, pitching and plunging aerofoils helicopter rotor blades, wind turbines etc. Here, the solver has been applied to study the effect of various parameters on flapping motion of NACA 0012 aerofoil and compared with available results of Isogai et al. and Tuncer et al.

Results

Here, NACA 0012 aerofoil is undergoing combined pitching and plunging motion sinusoidally is considered at different motion parameters. The C-H grid of size 247 × 65 around the aerofoil has been generated using commercial software GRIDGEN. The grid points are properly clustered near the leading edge, trailing edge and along wall normal direction which is shown in Fig. 1(a) and (b).

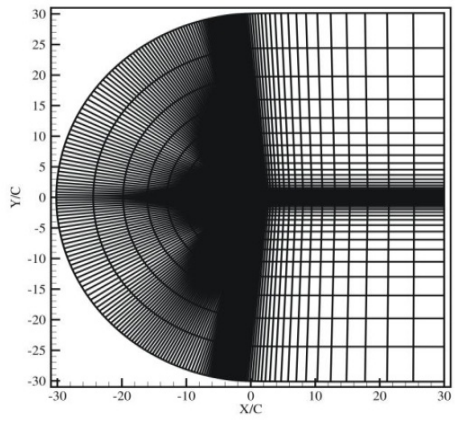

FIG. 1(a) C-H GRID AROUND NACA0012 AEROFOIL

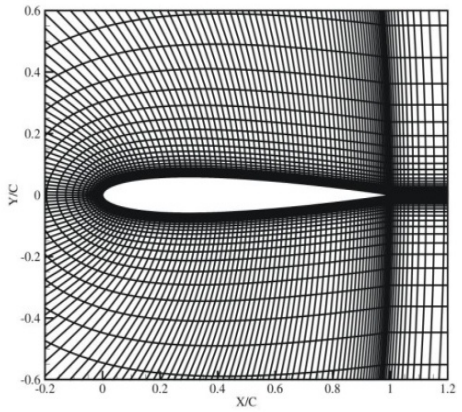

FIG. 1(b) CLOSE UP VIEW OF GRID

The combined pitching and plunging oscillation of an aerofoil is shown in Fig. 2. The plunging motion is defined as the vertical motion at right angles to the direction of uniform free stream velocity U_∞. The NACA 0012 aerofoil with chord length c performs a sinusoidal plunging. The position of the aerofoil is $y(t)$ given by

$$y(t) = y_o \sin(\omega t) \tag{8}$$

where t is physical time, ω the angular frequency.

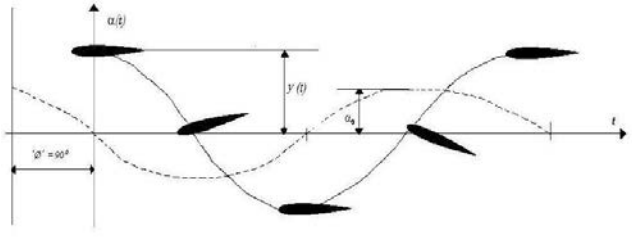

FIG. 2 AEROFOIL IN COMBINED PITCHING AND PLUNGING MOTION WITH A PHASE DIFFERENCE OF $\Phi = 90°$

Plunge amplitude, y_o, is positive in the upward direction and the reduced frequency is given by, $k = \omega c / U_\infty$.

The instantaneous non-dimensional plunging velocity is

$$\dot{y}/U_\infty = h_a k \cos(\omega t) \tag{9}$$

where the dot denotes a differentiation with respect to t and the non-dimensional plunge amplitude is $h_a = y_o / c$.

The instantaneous effective angle of attack due to pure plunging is

$$\alpha = \alpha_0 \sin(\omega t + \phi) \tag{10}$$

where the amplitude of pitching oscillation is α_0, ϕ is the phase angle ahead of the plunging motion which is also shown in Fig. 2. The instantaneous lift and thrust coefficients are C_l and C_t, respectively. The instantaneous pitching moment coefficient around the pitching-pivot point is C_m (positive in the nose-up sense).

The instantaneous input power co-efficient is

$$C_p = -(C_l \dot{y} + C_m c \dot{\alpha}) / U_\infty \tag{11}$$

The time-averaged lift coefficient, pitching moment coefficient, thrust coefficient and input power coefficient over an oscillation period are C_l, C_m, C_t and C_p respectively. The mean thrust coefficient is therefore defined as

$$(\overline{C_t}) = -\overline{C_d} + (C_d)_{steady} \tag{12}$$

where C_d is the mean drag coefficient, averaged for one flapping period. $(C_d)_{steady}$ is the steady drag of the non-moving wing at its present mean angle of attack.

The propulsive efficiency is calculated from the ratio between power output and power input. If dimensionless coefficients are used, this is equal to the ratio of mean thrust coefficient to mean power input coefficient

$$(\eta_{prop}) = (\overline{C_t}) / (\overline{C_p}). \tag{13}$$

As it can be identified from Fig. 2, the combined motion produces wave motion propagating in the x-direction. It is clear that the origin of this wave motion can be attributed to the coupled heaving and pitching oscillations with a finite phase difference. When we define the propagation velocity of the wave, the ratio of wave velocity to free stream velocity depends on the critical reduced frequency which in turn is a function of pivot point a, α_0 / h_a and φ. However, the behaviour of critical reduced frequency is still useful to select the parameters such as k, φ, h_a and α_0 for

which the numerical simulations are to be performed for various combinations of k and φ. For this reason, the behaviour of critical reduced frequency is studied or simulated for the following two different plunge amplitudes (h_a),

1. $h_a = 1.0$, $\alpha_0 = 20°$, $a = 0$, $M = 0.3$ and $R_e = 1.0 \times 10^5$

2. $h_a = 2.0$, $\alpha_0 = 10°$, $a = 0$, $M = 0.3$ and $R_e = 1.0 \times 10^5$

The present numerical simulations have been performed for various combinations of k and Φ for each of these two cases.

1. $h_a = 1.0$, $\alpha_0 = 20°$, $a = 0$, $M = 0.3$ and $R_e = 1.0 \times 10^5$

Table 1 shows the results optimized for maximum propulsion efficiency, η_P and time-averaged thrust coefficient, $\overline{C}_t$, respectively with respect to k for $\varphi = 90°$, which have been compared with Navier-Stokes results available in Isogai et al. The highest propulsion efficiency of 79.8% with a time-averaged thrust coefficient of 0.310 and the highest time-averaged thrust coefficient of 0.6118 with propulsion efficiency 43.10% are obtained. Fig. 3 shows the coefficient of lift, drag and moment versus the angle of attack for the final converged cycle. The pressure contours are shown in Fig. 4.

TABLE 1 COEFFICIENT OF THRUST AND PROPULSION EFFICIENCY FOR A PITCHING-PLUNGING NACA 0012 AEROFOIL

k	Coefficient of thrust		Propulsive efficiency × 100	
	Present (RANS)	Isogai [6]	Present (RANS)	Isogai [6]
0.5	0.10090528	0.310	0.79840	0.725
0.6	0.20012392	0.466	0.78002	0.6994
0.7	0.31576321	0.524	0.75058	0.6742
0.8	0.44585174	0.566	0.70883	0.6205
0.9	0.51040155	0.595	0.53349	0.5815
1.0	0.57188636	0.6118	0.43102	0.500

2. $h_a = 2.0$, $\alpha_0 = 10°$, $a = 0$, $M = 0.3$ and $R_e = 1.0 \times 10^5$

Table 2 and Table 3 show propulsion efficiency (η_P) and time-averaged thrust coefficient ($\overline{C}_t$) respectively which are compared against φ with k as a varying parameter compared to the available results obtained by Isogai et al. and Tuncer et al. both of who used a Navier-Stokes code with Baldwin and Lomax turbulence model. Although the agreements between the two computations are fairly good for $\varphi \geq 60°$, the large quantitative discrepancies are seen in both η_P and C_t for $\varphi = 30°$, in which case, the severe leading edge-flow separations have been observed in our computations for all of the reduced frequencies computed, whereas no flow separation has been observed for $k = 0.15$ in the computations by Tuncer and Platzer. It is interesting to see their results that the highest $\overline{C}_t$ is obtained for $k = 0.15$ and $\varphi = 60°$. It is clear that the low values of $\overline{C}_t$ and poor efficiency obtained for $k = 0.5$ can be attributed to the occurrence of large-scale leading-edge separation. The highest propulsion efficiency of 95.14% with a time-averaged thrust coefficient of 0.0875 and the highest time-averaged thrust coefficient of 0.3168 with propulsion efficiency 19.09% are obtained. Fig. 5 shows the coefficient of lift, drag and moment versus the angle of attack for the final converged cycle. The Mach number contour at different instants of time for one complete cycle of flapping motion of the aerofoil is plotted in Figs. 6. The critical flow patterns are well captured and flow separations are seen clearly in the plots. There is a difference in predicted propulsion efficiency and time-averaged thrust coefficient values and that of Isogai et al. at smaller reduced frequencies is probably due to the presence of viscous effects.

TABLE 2 COEFFICIENT OF THRUST FOR A PITCHING-PLUNGING NACA 0012 AEROFOIL

φ	k	Coefficient of thrust		
		Present RANS	Isogai [6]	Tuncer [16]
30°	0.15	0.1267	0.1	1.4
	0.3	0.01601	0.03	0.32
	0.5	0.0178	0.04	0.1
60°	0.15	0.112166	0.71	1.325
	0.3	0.131885	0.5	0.5989
	0.5	0.17113	0.26	0.34
90°	0.15	0.08750	0.88	1.015
	0.3	0.21918	0.706	0.752
	0.5	0.28837	0.415	0.41
120°	0.15	0.08895	0.66	0.72
	0.3	0.212377	0.74	0.725
	0.5	0.316890	0.409	0.389
150°	0.15	0.1061	0.665	0.66
	0.3	0.14267	0.4401	0.492
	0.5	0.25199	0.26	0.2599

TABLE 3 PROPULSION EFFICIENCY FOR A PITCHING-PLUNGING NACA 0012 AEROFOIL

φ	k	Propulsive efficiency × 100		
		Present RANS	Isogai [6]	Tuncer [16]
30°	0.15	0.8098	0.05	0.64
	0.3	0.03405	0.036	0.15
	0.5	0.01265	0.05	0.089
60°	0.15	0.931473	0.556	0.72
	0.3	0.271101	0.2722	0.32
	0.5	0.11772	0.142	0.164
90°	0.15	0.95145	0.787	0.832
	0.3	0.40189	0.406	0.432
	0.5	0.18597	0.215	0.22
120°	0.15	0.81822	0.765	0.865
	0.3	0.37524	0.391	0.42
	0.5	0.19096	0.198	0.201
150°	0.15	0.6952	0.62	0.72
	0.3	0.2024	0.1982	0.2535
	0.5	0.1441	0.1	0.152

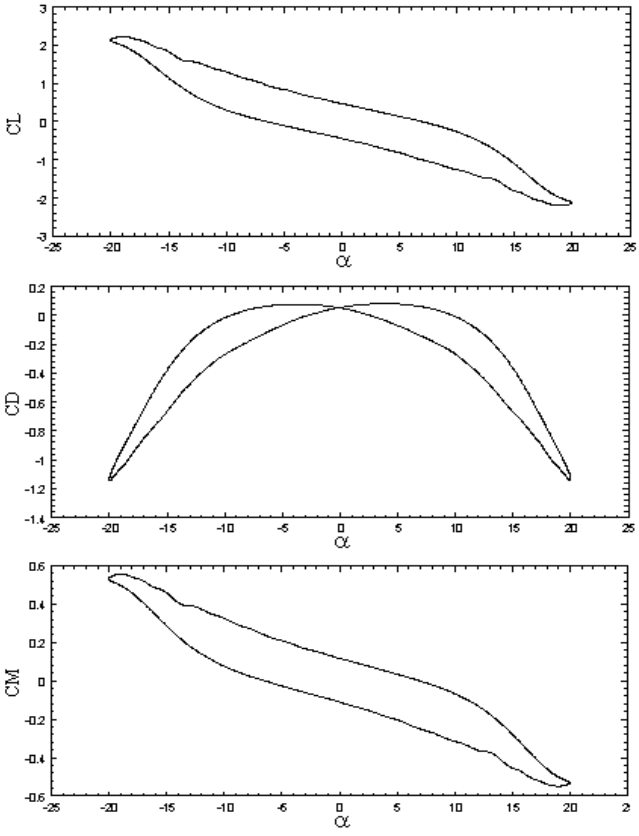

FIG. 3 THE COEFFICIENT OF LIFT, DRAG AND MOMENT VERSUS THE ANGLE OF ATTACK FOR THE FINAL CYCLE AT h_a = 1.0, α_0 = 20°, a = 1/2, M = 0.3, k = 0.9 and ϕ = 90°

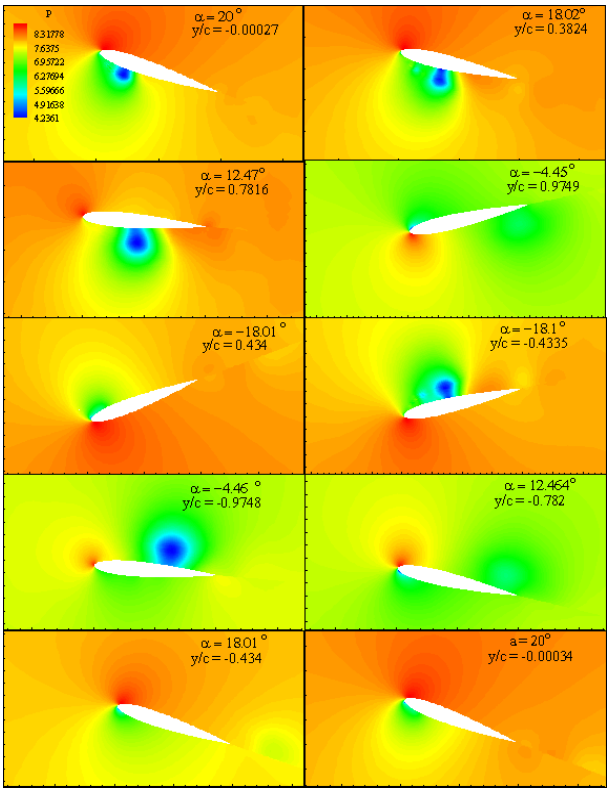

FIG. 4 THE PRESSURE FIELDS AT DIFFERENT INSTANTS OF TIME FOR ONE CYCLE OF FLAPPING MOTION OF AEROFOIL AT h_a=1.0, α_0 = 20°, a = 1/2, M = 0.3, k = 0.9 and φ = 90°

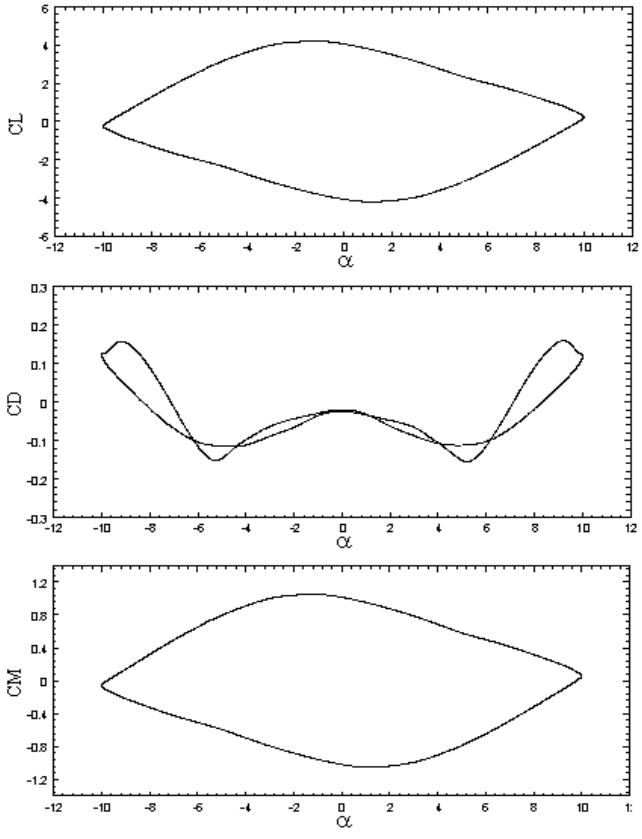

FIG. 5 THE COEFFICIENT OF LIFT, DRAG AN D MOMENT VERSUS THE ANGLE OF ATTACK FOR THE FINAL CYCLE AT h_a = 2.0, α_0 = 10°, a = 1/2, M = 0.3, k = 0.5 and φ = 30°

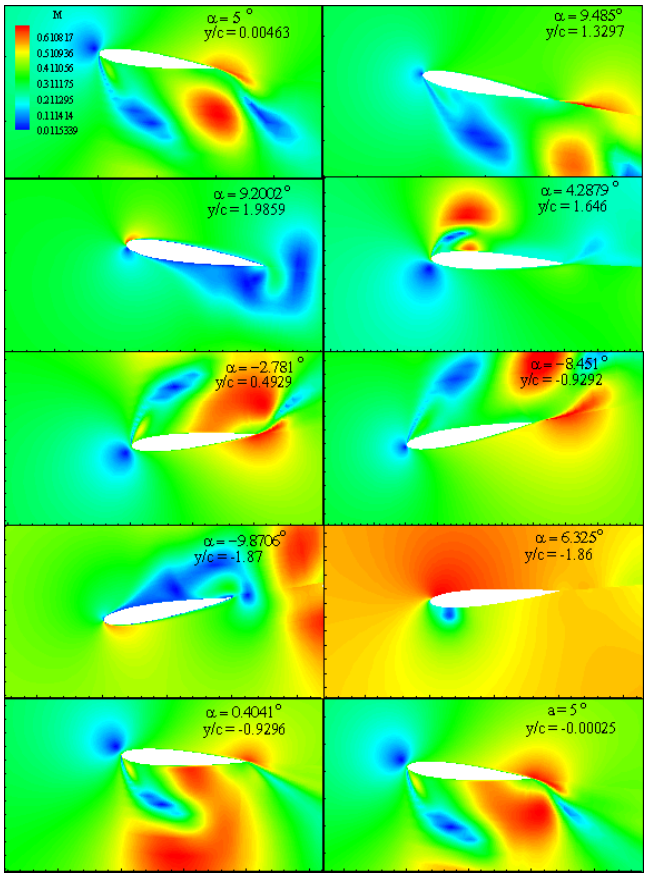

FIG. 6: THE MACH CONTOURS AT DIFFERENT INSTANTS OF TIME FOR ONE CYCLE OF FLAPPING MOTION OF AEROFOIL AT h_a = 2.0, α_0 = 10°, a = 1/2, M = 0.3, k = 0.5 and φ = 30°

Conclusions

The time-averaged thrust coefficient of a combined pitching-plunging NACA 0012 aerofoil computed by the RANS solver agrees fairly well with those obtained by Navier-Stokes solutions in the literature. The effect of various motion parameters on the time-averaged thrust generation and propulsive efficiency has been studied. The highest propulsive efficiency and the highest thrust coefficient do not occur at the same reduced frequency. Higher propulsive efficiency usually occurs at lower reduced frequency, where as higher thrust occurs at higher reduced frequency. As the flow becomes more and more unsteady with increasing reduced frequency, a large amount of vorticity is shed from the trailing edge. At higher values of pitching amplitude time histories of the coefficient of lift, thrust, drag and moment are smooth purely sinusoidal but, as the pitching amplitude is decreased, the time histories of these coefficients are not sinusoidal as their shape is deformed thus resulting in the decrease in propulsion efficiency and an increase in the thrust coefficient comparatively. The maximum propulsive efficiency and minimum thrust for the range of cases considered in the present study occur when the phase angle between pitching and plunging motion is approximately 90°.

REFERENCES

Anderson, J. M., "Vorticity control for efficient propulsion", PhD Thesis, Massachusetts Institute of Technology and Woods Hole Oceanographic Institution, 1996.

Anderson, J. M., Streitlien, K., Barrentt D. S. and Triantafyllou, M. S., "Oscillating foils of high propulsive efficiency", *J. Fluid Mech*., Vol. 360, pp. 41–72, 1998.

Baldwin B. S. and Lomax, H. "Thin layer approximating and algebraic model for separated turbulent flows", AIAA Paper 78-275, 1978.

Beam R. M. and Warming, R. F., "An Implicit Factored Scheme for the Compressible Navier-Stokes Equations", *AIAA Journal*, Vol. 16, No. 4, pp. 393 – 402, 1978.

Dutta, P. K., Vimala Dutta and Sharanappa V. Sajjan, "RANS Computation of Flow past Wind Turbine Blades", Proc., of 7th Asian Computational Fluid Dynamics Conference, Bangalore, 26th – 30th November, 2007 (Invited Paper).

Garrick, I. E., "Propulsion of a flapping and oscillating Aerofoil", NACA REPORT No. 567, May 1936.

Hall, M. G., "Cell Vertex Multi-grid Scheme for Solution of the Euler Equations", RAE-TM-Aero 2029, Proc. Conf. on Numerical methods for fluid dynamics, pp. 303 – 345, 1985.

Ho C. M. and Chen, S.H., "Unsteady wake of a plunging Aerofoil", *AIAA Journal*, Vol. 19, pp. 1492–1494, 1981Roy. "Unsteady Aerodynamics", Proc. Two Day Conf., Aero. Soc., London, 17- 18 July 1996.

Isogai, K., Shinmoto Y. and Watanabe, Y., "Effects of dynamic stall on propulsive efficiency and thrust of flapping Aerofoil", *AIAA Journal*, Vol. 37, pp. 1145–1151, 1999.

Jameson, A., Schmidt W. and Turkel, E., "Numerical Solution of Euler Equations by Finite Volume Methods Using Runge Kutta Time Stepping Schemes", AIAA Paper 81 – 1259, 1981.

Sharanappa V. Sajjan, Vimala Dutta and Dutta, P. K., "Numerical Simulation of Flow over Pitching Bodies using an implicit Reynolds-averaged Navier-Stokes Solver", Proc. of 12th Asian congress of Fluid Mechanics, Daejeon, Korea, 18th – 21st, August 2008.

Sharanappa V. Sajjan, Vimala Dutta and Dutta, P. K., "Viscous Unsteady Flow around a Helicopter Rotor Blade in Forward Flight", Proc., 9th Annual CFD Symposium, CFD Division of Aeronautical Society of India, Bangalore, August 11-12, 2006.

Siva Kumar K. and Sharanappa V. Sajjan, "Numerical Simulation of Unsteady Flow over a Plunging Aerofoil Using an Implicit Reynolds averaged Navier-Stokes Solver", NAL PD CF 1003, March 2010.

Siva Kumar K. and Sharanappa V. Sajjan, "Unsteady Flow past a Combined Pitching and Plunging Aerofoil using an Implicit RANS Solver", *Applied Mechanics and Materials*, Vol. 110 - 116, pp. 3481-3488, 2012.

Theodorsen, T., "General theory of aerodynamic instability and the mechanism of flutter", NACA REPORT No. 496, May 1934.

Tuncer, I. H., Walz, R. and Platzer, M., "A computational study on the dynamic stall of a flapping Aerofoil", AIAA Paper 1998-2519, June 1998.